

Pulsar wind nebulae of runaway massive stars

Meyer, D. M.-A.¹ and Meliani, Z.²

¹ Institut für Physik und Astronomie, Universität Potsdam, Karl-Liebknecht-Strasse 24/25, D-14476 Potsdam, Germany,
E-mail: dnameyer.astro@gmail.com

² Laboratoire Univers et Théories, Observatoire de Paris, Université PSL, Université de Paris, CNRS, F-92190 Meudon, France
E-mail: zakaria.meliani@observatoiredeparis.psl.eu

Last updated 2020 June 10; in original form 2013 September 5

ABSTRACT

A significant fraction of massive stars move at speed through the interstellar medium of galaxies. After their death as core-collapse supernovae, a possible final evolutionary state is that of a fast-rotating magnetised neutron star – shaping its circumstellar medium into a pulsar wind nebula. Understanding the properties of pulsar wind nebulae requires knowledge of the evolutionary history of their massive progenitors. Using two-dimensional magneto-hydrodynamical simulations, we demonstrate that, in the context of a runaway high-mass red-supergiant supernova progenitor, the morphology of its subsequent pulsar wind nebula is strongly affected by the wind of the defunct progenitor star pre-shaping the stellar surroundings throughout its entire past life. In particular, pulsar wind nebulae of obscured runaway massive stars harbour asymmetries function of the morphology of the progenitor’s wind-blown cavity, inducing projected asymmetric up-down synchrotron emission.

Key words: methods: MHD – stars: evolution – stars: massive – pulsars: general – ISM: supernova remnants.

1 INTRODUCTION

About 10%–25% of OB-type massive stars are runaway objects (Blaauw 1961; Schoettler et al. 2022) with peculiar supersonic speeds with respect to their interstellar medium (ISM). Two main mechanisms are proposed to explain the production of such runaway stars, namely binary-supernova ejection and dynamical ejection from the stellar cluster (Hoogerwerf et al. 2000) and their trajectory can be traced back to their parent starburst regions (Schoettler et al. 2019). These massive stars die as core-collapse supernovae releasing most of the remaining stellar mass with high speed into the surrounding circumstellar medium (CSM) before expanding into the ISM.

Often, at the location of the supernova explosion, remains a highly-magnetised and fast-rotating neutron star (pulsar). The pulsar generates a powerful wind with a kinetic luminosity that can reach $\dot{E} \sim 10^{39} \text{ erg s}^{-1}$ inducing a growing pulsar wind nebula (PWN). This PWN evolves first into the freely-expanding supernova ejecta before reaching the supernova reverse shock (Blondin et al. 2001). After it interacts with the swept-up CSM and, at a later time, with the unshocked ISM.

Previous investigations on PWN of moving pulsar concentrate on the birth kick pulsar. It occurs when massive stars collapse (de Vries et al. 2021). The resulting pulsar propagates through the supernova ejecta (Slane et al. 2018). On timescales of a few kyr, the fast-moving pulsar escapes the supernova remnant (SNR) and travels in the uniform and cold ISM (Barkov et al. 2019; Bucciantini et al. 2020). The resulting PWN morphology is strongly deformed and develops an extended tail. Because of numerical and physical difficulties associated with the CSM modelling, the simulations of PWN are mainly performed in classical hydrodynamics and deal only with moving pulsars inside supernova ejecta (Temim et al. 2015, 2022). Rela-

tivistic simulations have been performed for pulsars moving in the ISM (Barkov et al. 2019; Bucciantini et al. 2020), while others also deal with static pulsar wind expanding into the supernova ejecta in 1D and 2D (Blondin et al. 2001; van der Swaluw et al. 2003; van der Swaluw 2003; van der Swaluw et al. 2004; Slane et al. 2018). However, these works did not account for all the evolution phases of the stellar progenitor of the runaway pulsar.

For pulsars from massive runaway stars, their wind mainly expands in the supernova remnant (SNR) constituted of supernova ejecta and CSM materials. Thus, shocks and instabilities, as well as the overall PWN morphology will be affected by these structures. Since SNRs are strongly affected by the CSM distribution (Cox et al. 2012), the PWNs and the properties of the various shocks therein should be, in their turn, a function of their surrounding CSM. Most common runaway massive stars shape the CSM with a large amount of red supergiant material as dense asymmetric stellar wind bow shocks (Cox et al. 2012; Henney & Arthur 2019a,b,c; Meyer et al. 2020a; Herbst et al. 2022), it should not be omitted in the modelling of their PWNs.

Motivated by the above arguments, we numerically investigate the shaping of PWN of fast-moving massive core-collapse supernova progenitor. We focus on the particular effects of the CSM generated by the wind-ISM interaction of the progenitor star. This study is organised as follows. First, we present the numerical methods used to model the pulsar wind nebula of a runaway massive progenitor star in Section 2. The outcomes of the simulations are presented in Section 3. We discuss our results and draw our conclusions in Section 4.

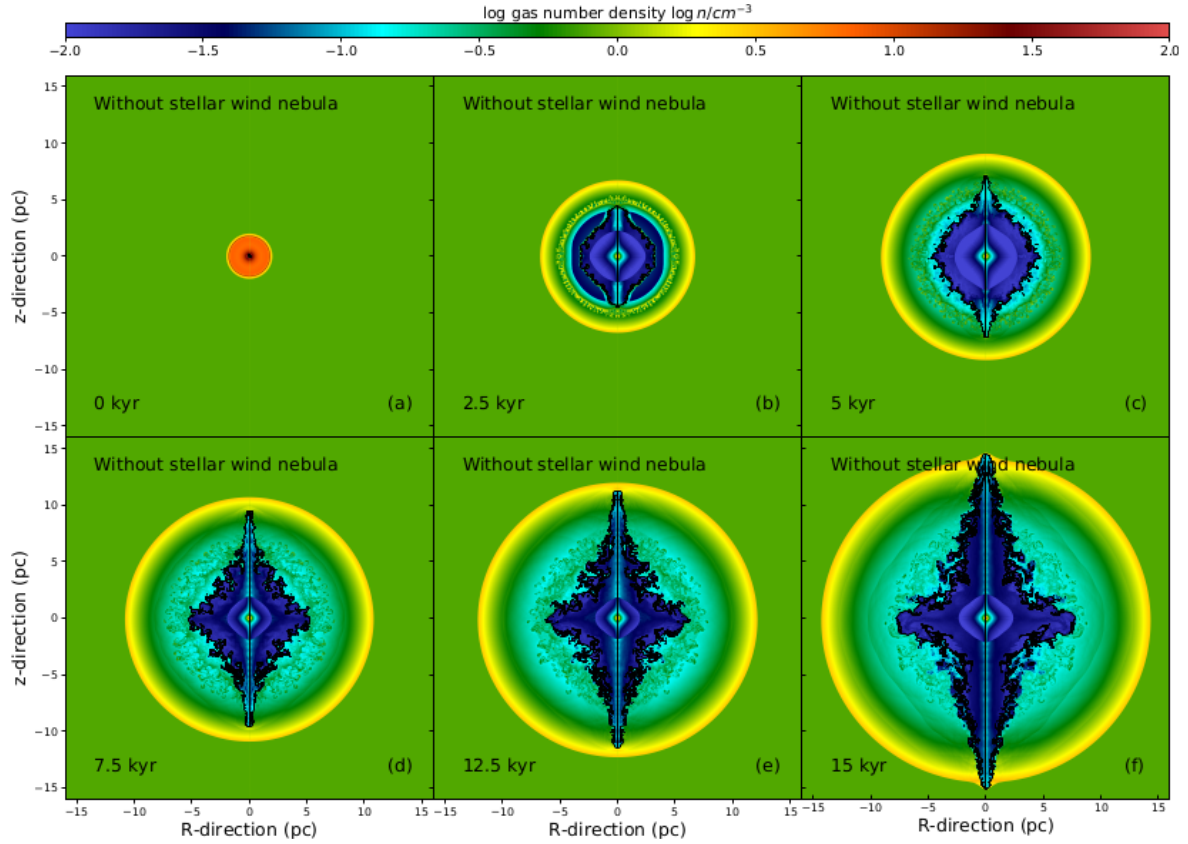


Figure 1. Time evolution of the number density field (in cm^{-3}) in the simulation of the nebula generated by a pulsar wind injected into the expanding ejecta of a core-collapse supernova. The black contour marks the region of the nebula made of 50% of pulsar wind material in number density. Time is measured starting from the onset of the pulsar wind.

2 METHOD

This study focuses on the entire evolution of the circumstellar medium of a runaway $20 M_{\odot}$ star at Galactic metallicity. The stellar surface properties such as wind velocity and mass-loss rate histories are taken from a model of the *GENEVA* evolutionary tracks library calculated without rotational mixing (Eldridge et al. 2006; Ekström et al. 2012).

We model the stellar surroundings from the zero-age main-sequence to the pre-supernova phase, through its red supergiant phase. When the star achieves its evolution, we inject therein supernova core-collapse ejecta made of mass $M_{\text{ej}} = 6.96 M_{\odot}$ and energy $E_{\text{ej}} = 10^{51} \text{ erg}$, using a density power-law profile (Whalen et al. 2008; Meyer et al. 2020a). The pulsar wind is modelled according to Komissarov & Lyubarsky (2004), using a wind power $\dot{E}_0 = 10^{38} \text{ erg s}^{-1}$, a wind velocity $10^{-2}c$ with c the speed of light in vacuum, a pulsar spin $P_0 = 0.3 \text{ s}$, a spin period variation $\dot{P}_0 = 10^{-17} \text{ s s}^{-1}$ and a wind magnetisation parameter $\sigma = 10^{-3}$ (Slane 2017). The pulsar loses energy according to an initial spin-down time scale $\tau_0 = P_0 / ((N-1)\dot{P}_0)$, where the braking index $N = 3$ stands for magnetic dipole spin-down. The energy diminution equations therefore reads $\dot{E}(t) = \dot{E}_0 (1+t/\tau_0)^{\alpha}$ with $\alpha = -(N+1)/(N-1)$, see Pacini & Salvati (1973). In this first paper, we run 2.5D simulations. Therefore, it is assumed that the spin axis and the direction of motion of the star coincide with the axis of symmetry of the cylindrical coordinate system.

The massive star moves through the ISM of the Milky Way's galactic plane of initial gas density 0.79 cm^{-3} and temperature of

8000 K (Wolfire et al. 2003; Meyer et al. 2014). We adopt an undisturbed ISM magnetic field parallel to direction of motion of the star with a strength of $7 \mu\text{G}$ which corresponds to a Alfvén speed of $v_A = 17.2 \text{ km s}^{-1}$ (Meyer et al. 2017).

The 2.5D numerical magneto-hydrodynamical simulations are performed with the code *PLUTO* (Mignone et al. 2007, 2012). We make use of the Godunov-type numerical scheme HLL Riemann solver combined with the PPM limiter, together with a third-order Rung-Kutta time-marching algorithm controlled by the Courant-Friedrich-Levi number. As in van der Swaluw et al. (2003), we set the polytropic index to $5/3$ and optically-thin radiative cooling physics is used for all circumstellar evolutionary phases except starting from the onset of the pulsar wind. More precisely, we make use of the optically-thin cooling and heating curves for fully ionized medium (Wiersma et al. 2009) of solar abundance (Asplund et al. 2009) presented in Meyer et al. (2014). Calculations are conducted following a mapping strategy (van Marle et al. 2015; Meyer et al. 2020a, 2021) in which the progenitor's CSM is first calculated, before supernova ejecta and eventually pulsar wind are injected into it. The models are conducted using a cylindrical coordinate system (R, z) that is mapped with a uniform mesh $[0, 150] \times [-50, 50]$ of spatial resolution $1.2 \times 10^{-2} \text{ pc cell}^{-1}$ for the CSM and a mesh $[0, 20] \times [-20, -20]$ of resolution $6.7 \times 10^{-3} \text{ pc cell}^{-1}$ for the PWN. The central sphere in which winds are imposed is of radius 20 cells (0.24 pc during the stellar wind phase and 0.134 pc throughout the pulsar phase).

Two simulations are performed with a runaway star of space velocity $v_{\star} = 40 \text{ km s}^{-1}$ (Mach number $\mathcal{M} \sim 4$). The first one considers

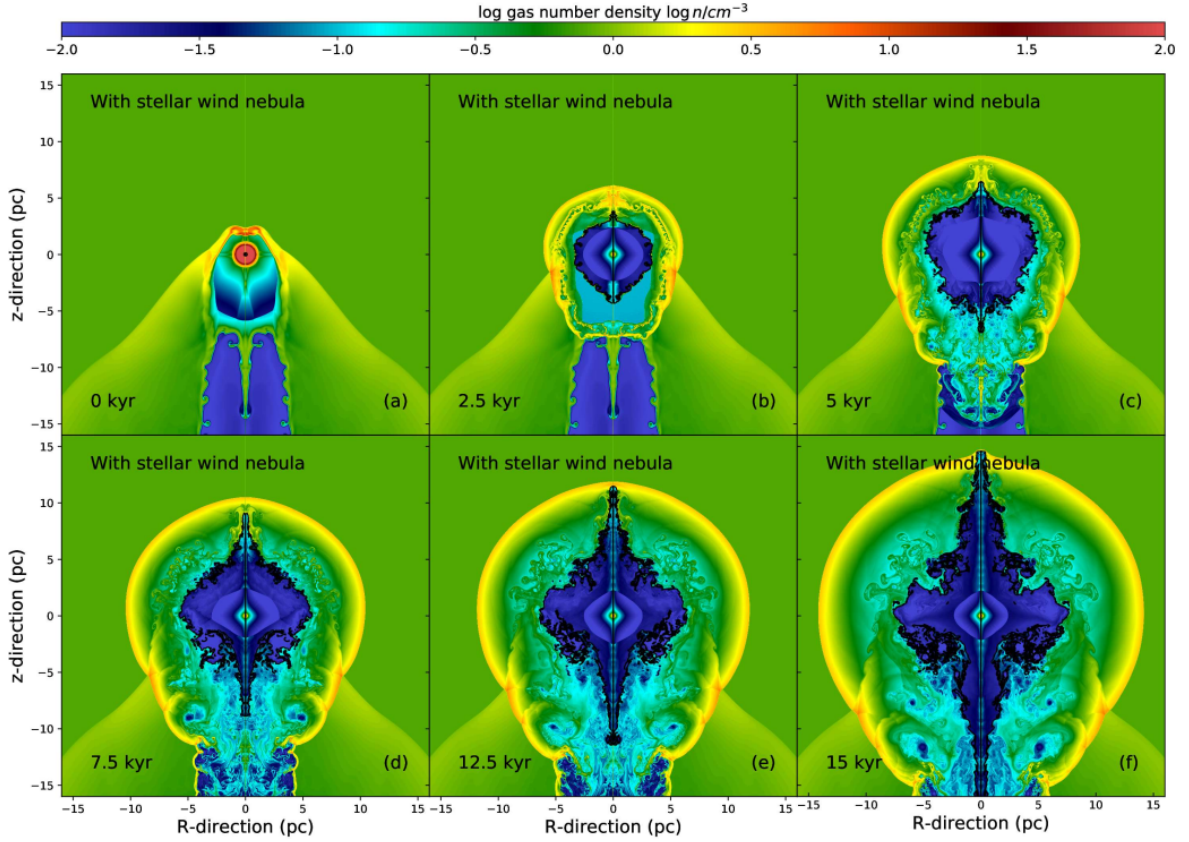


Figure 2. As for Fig. 1, with the presence of the circumstellar medium (CSM) generated by the wind-ISM interaction of the $20 M_{\odot}$ massive runaway progenitor.

the pulsar wind expanding into supernova ejecta only, while the second one also accounts for the progenitor’s CSM.

3 RESULTS

3.1 Model without wind-ISM interaction

For the sake of comparison, we first model a PWN accounting for core-collapse supernova ejecta but neglecting the CSM, the entire system being in supersonic motion in the ambient medium. The time sequence evolution of the number density field of such system is displayed in Fig. 1.

The pulsar wind is set in the dense supernova ejecta which has expanded up to a few pc into the local ISM (Fig. 1a). About 2.5 kyr later, the PWN has adopted a structure made of the freely-expanding pulsar wind, a PWN termination shock, a PWN/ejecta inner contact discontinuity (black contour) and a transmitted PWN forward shock propagating into the unshocked supernovae ejecta. The ejecta-ISM interaction leads to the formation of an outer ejecta-ISM contact discontinuity affected by strong Richtmyer-Meshkov instabilities (Kane et al. 1999), while a reflected supernova termination shock forms and propagates inwards heating the pulsar wind. Meanwhile, the supernova forward shock propagates through the ISM (Fig. 1b).

The system keeps on growing in size over the next few kyr, revealing an efficient mixing of pulsar and ejecta materials. The magnetised pulsar wind develops a bipolar jet along its rotation axis, see black contours of Fig. 1c. At time 7.5 kyr the PWN harbors an equatorial disc-like feature, normal to the bipolar jet which has gone through the unstable region where the mixing of materials takes

place and it penetrates the outer layer of shocked ISM gas of the SNR (Fig. 1d). The magnetised PWN, at this point, displays the typical cross-like anisotropic morphology described in Komissarov & Lyubarsky (2004), embedded by an overall spherically-symmetric expanding blastwave (Fig. 1e). Last, the jet of the pulsar catches up the supernova remnant shock wave and begins to expand into the ISM, generating polar bow shocks (Fig. 1f).

During the evolution, the supernova ejecta high speed compensates the ISM ram pressure, allowing the SNR, and, consequently, the PWN morphology to conserve an isotropic symmetry.

3.2 Effects of the progenitor’s wind-ISM interaction

In the second model, all evolution stages of the massive progenitor are considered before the supernova explosion occurs and the pulsar starts blowing into the former stellar wind (Fig. 2). The gas distribution at the onset of the pulsar wind is complex, as the wind-ISM interaction shaped it throughout the previous star’s life. Its arc-like nebula is composed of the large-scale component produced by the main-sequence stellar wind plus the shell of red supergiant wind that has been subsequently released in it (Meyer et al. 2014). The pre-pulsar CSM is therefore a central region of expanding ejecta surrounded by a low-density cavity opposite of, with a high-density bow shock facing the direction of the progenitor’s motion (Fig. 2a), see also Meyer et al. (2015, 2021). The asymmetric propagation of the supernova blastwave is strongly constrained by the walls of the cavity. It is channelled by the cavity in the direction opposite of that of the stellar motion shock has gone through the CSM (Fig. 2b).

The global organisation of the SNR and its central PWN exhibits

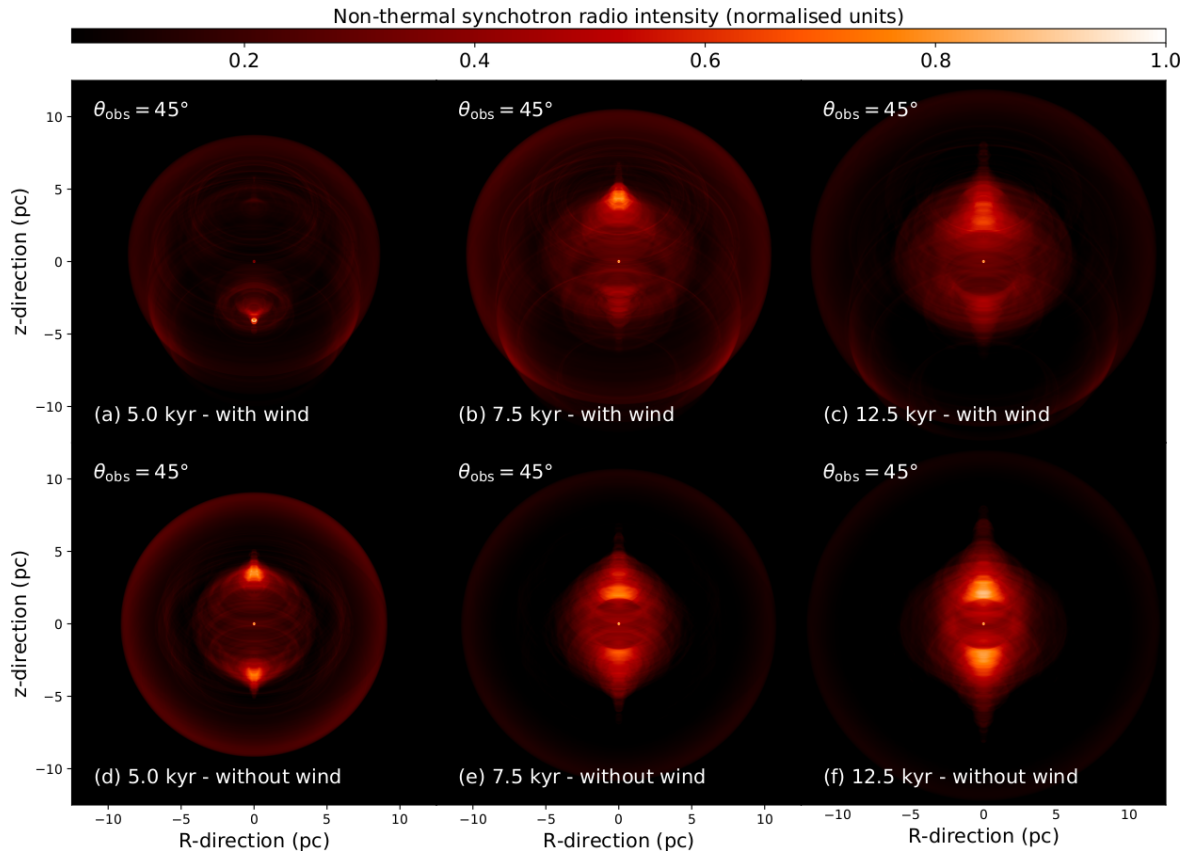


Figure 3. Selected time sequence evolution of synchrotron emission map assuming an angle $\theta_{\text{obs}} = 45^\circ$ between the observer’s line-of-sight and the axis of symmetry of the nebula. The images compare models with (top) and without (bottom) the stellar wind of the massive progenitor.

qualitative dissimilarities to that of Fig. 1 as the game of shock reflections generates a more complex object. The morphology of the pulsar wind-ejecta interface is governed by that of the ejecta region, adopting its ovoidal shape (Fig. 2c) different to that of the model without the progenitor’s stellar wind (Fig. 1c). At the time 7.5 kyr, the supernova ejecta are channelled into the tubular region of shocked stellar wind generated by the progenitor’s motion and the pulsar wind develops a bipolar jet, although the pulsar wind remains equatorially asymmetric (Fig. 2d). The nebula further evolves such that the inner contact discontinuity of the PWN shapes as a function of (i) the pulsar magneto-rotational properties and (ii) the supernova shock wave material that is reflected towards the center of the explosion. Finally, the contact discontinuity recovers the overall morphology of a bipolar jet normal to an equatorial structure (Fig. 2e), with important persisting equatorial dissymmetries (Fig. 2f).

4 DISCUSSION AND CONCLUSION

In this paper, we numerically investigate, in the context of a runaway massive supernova progenitor and within the frame of the ideal magneto-hydrodynamics, the influences of the CSM shaped during all the progenitor’s evolutionary stages on the long-term (\sim kyr) morphological development of the PWN after the pulsar birth and on the instabilities growing at shocks. Other works concerning the release of pulsar winds in SNR were set in the frame of ideal hydrodynamics (Blondin et al. 2001; van der Swaluw et al. 2003; van der Swaluw 2003; van der Swaluw et al. 2004; Slane et al. 2018) as well as magneto-hydrodynamics, see Olmi & Torres (2020) and

references therein. Nevertheless, if some studies tackle the problem of runaway pulsars (Olmi & Bucciantini 2019), or even investigated the effects of a stratified ISM (Kolb et al. 2017), none of them include in detail the stellar wind feedback of the core-collapse progenitor. In our scenario, the pulsar wind-supernova ejecta system is embedded into a dense CSM, where a large part of the progenitor mass lays, released as pre-supernova stellar wind. Note that our models assume that the pulsar is static in the frame of reference of the runaway star, so we are neglecting the birth kick that many pulsars receive from the supernova explosion. Assuming a typical kick velocity of $\approx 400 \text{ km s}^{-1}$ (Verbunt et al. 2017), the pulsar would be displaced by about 6 pc over the 15 pc that we simulate. Therefore our results apply mainly to the low-velocity pulsar sub-population ($\leq 50 \text{ km s}^{-1}$), which comprises $\approx 2 - 5\%$ of all pulsars (Igoshev 2020).

Our study shows, in the particular context of a fast-moving red supergiant star in the Galactic plane, that the wind-blown bubble of a core-collapse supernova progenitor has a governing impact on the morphology of its subsequent PWN. As early as ~ 2.5 kyr, the distribution of the contact discontinuity between magnetised pulsar wind and supernova ejecta adopts an oblong shape as a result of the anisotropic ejecta distribution. Since core-collapse SNRs shape according to their CSM, PWNs similarly take their morphology as a direct consequence of their progenitor’s stellar evolution history. Because a significant fraction of massive stars are runaway objects, our findings imply that the stellar wind history should not be neglected in the understanding of PWN and that the CSM-induced asymmetries should account for up to 10%–25% of all individual PWNs.

The stellar wind history that we use is that of a $20 M_\odot$ supergiant

star which is amongst the most common progenitors of core-collapse SNRs (Katsuda et al. 2018), although higher-mass evolutionary channels might exist, i.e. involving Wolf-Rayet progenitors. The bulk motion of the star is taken to be within that of the most common runaway stars (Blaauw 1993). However, a small fraction of high-mass stars move with (Lennon et al. 2018) and might form PWNs for which the influence of the CSM is milder. Given that the morphology of PWNs retains information from the stellar evolution history of massive stars, our model applies to objects in the Galactic disc region ($\sim 1 \text{ cm}^{-3}$) rather than in the high-latitude parts of the Milky Way, where the low-density medium induce an extended CSM (Meyer et al. 2020b) with which supernova shock waves (and eventually pulsar winds) weakly interact. Conversely, massive stars running through dense molecular regions are more prone to form complex CSM, and, therefore, to produce very asymmetric PWNs.

We generate predictive images for our asymmetric PWN from a runaway massive star. Fig. 3 plots non-thermal radio synchrotron emission maps using the emissivity $\propto p B_{\perp}^{(s+1)/2}$ with p the thermal pressure of the gas, B_{\perp} the component of the magnetic field along the observer's line-of-sight and $s = 2$ the power-law index of the non-thermal electrons distribution (Jun & Norman 1996). The images are produced with the RADMC-3D code (Dullemond 2012), displayed with (top) and without CSM (bottom), for selected time instances, and assuming an inclination angle of the pulsar is $\theta_{\text{obs}} = 45^\circ$ to the plane of the sky. The pulsar wind is at first not visible in the region facing the progenitor's direction of motion, where the supernova shock wave interacting with the wind bubble dominates (Fig. 3a,d). Once the pulsar polar jet grows and penetrates the dense region of stellar wind and ejecta, it becomes brighter than that in the cavity (Fig. 3b,c). This projected up-down surface brightness asymmetry increases with time, as the front jet starts to interact with the shocked supernova material and the other-side jet continues to propagate in the rarefied medium of the stellar wind cavity.

Our results show that the effects of the progenitor's stellar wind impacts the global morphology of PWNs, and, consequently it influences the properties of the shocks therein. This should significantly modify the injection and acceleration physics of the relativistic particle population, which, in their turn, are responsible for the non-thermal emission properties of the PWNs.

We intend to extend this work to a broader study investigating the parameter space of various massive stellar progenitors, relativistically treating the pulsar wind and including the kick received by pulsar.

ACKNOWLEDGEMENTS

The authors thank the referee, W. Henney, for advice which improved the quality of the paper. The authors acknowledge the North-German Supercomputing Alliance (HLRN) for providing HPC resources that have contributed to the research results reported in this paper.

DATA AVAILABILITY

The data underlying this article will be shared on reasonable request to the corresponding author.

REFERENCES

Asplund M., Grevesse N., Sauval A. J., Scott P., 2009, *ARA&A*, **47**, 481
Barkov M. V., Lyutikov M., Klingler N., Bordas P., 2019, *MNRAS*, **485**, 2041

- Blaauw A., 1961, *Bull. Astron. Inst. Netherlands*, **15**, 265
Blaauw A., 1993, in Cassinelli J. P., Churchwell E. B., eds, *Astronomical Society of the Pacific Conference Series Vol. 35, Massive Stars: Their Lives in the Interstellar Medium*. p. 207
Blondin J. M., Chevalier R. A., Frierson D. M., 2001, *ApJ*, **563**, 806
Bucciantini N., Olmi B., Del Zanna L., 2020, in *Journal of Physics Conference Series*. p. 012002 ([arXiv:2005.14079](#)), doi:10.1088/1742-6596/1623/1/012002
Cox N. L. J., Kerschbaum F., van Marle A.-J., Decin L., Ladjal D., Mayer A., 2012, *A&A*, **537**, A35
Dullemond C. P., 2012, RADMC-3D: A multi-purpose radiative transfer tool, *Astrophysics Source Code Library* (ascl:1202.015)
Ekström S., et al., 2012, *A&A*, **537**, A146
Eldridge J. J., Genet F., Daigne F., Mochkovitch R., 2006, *MNRAS*, **367**, 186
Henney W. J., Arthur S. J., 2019a, *MNRAS*, **486**, 3423
Henney W. J., Arthur S. J., 2019b, *MNRAS*, **486**, 4423
Henney W. J., Arthur S. J., 2019c, *MNRAS*, **489**, 2142
Herbst K., et al., 2022, *Space Sci. Rev.*, **218**, 29
Hoogerwerf R., de Bruijne J. H. J., de Zeeuw P. T., 2000, *ApJ*, **544**, L133
Igoshev A. P., 2020, *MNRAS*, **494**, 3663
Jun B.-I., Norman M. L., 1996, *ApJ*, **472**, 245
Kane J., Drake R. P., Remington B. A., 1999, *ApJ*, **511**, 335
Katsuda S., Takiwaki T., Tominaga N., Moriya T. J., Nakamura K., 2018, *ApJ*, **863**, 127
Kolb C., Blondin J., Slane P., Temim T., 2017, *ApJ*, **844**, 1
Komisarov S. S., Lyubarsky Y. E., 2004, *MNRAS*, **349**, 779
Lennon D. J., et al., 2018, *A&A*, **619**, A78
Meyer D. M.-A., Mackey J., Langer N., Gvaramadze V. V., Mignone A., Izzard R. G., Kaper L., 2014, *MNRAS*, **444**, 2754
Meyer D. M.-A., Langer N., Mackey J., Velázquez P. F., Gusdorf A., 2015, *MNRAS*, **450**, 3080
Meyer D. M.-A., Vorobyov E. I., Kuiper R., Kley W., 2017, *MNRAS*, **464**, L90
Meyer D. M. A., Petrov M., Pohl M., 2020a, *MNRAS*, **493**, 3548
Meyer D. M. A., Oskinova L. M., Pohl M., Petrov M., 2020b, *MNRAS*, **496**, 3906
Meyer D. M. A., Pohl M., Petrov M., Oskinova L., 2021, *MNRAS*, **502**, 5340
Mignone A., Bodo G., Massaglia S., Matsakos T., Tesileanu O., Zanni C., Ferrari A., 2007, *ApJS*, **170**, 228
Mignone A., Zanni C., Tzeferacos P., van Straalen B., Colella P., Bodo G., 2012, *ApJS*, **198**, 7
Olmi B., Bucciantini N., 2019, *MNRAS*, **488**, 5690
Olmi B., Torres D. F., 2020, *MNRAS*, **494**, 4357
Pacini F., Salvati M., 1973, *ApJ*, **186**, 249
Schoettler C., Parker R. J., Arnold B., Grimmert L. P., de Bruijne J., Wright N. J., 2019, *MNRAS*, **487**, 4615
Schoettler C., Parker R. J., de Bruijne J., 2022, *MNRAS*, **510**, 3178
Slane P., 2017, in Alsabti A. W., Murdin P., eds., *Handbook of Supernovae*. p. 2159, doi:10.1007/978-3-319-21846-5_95
Slane P., et al., 2018, *ApJ*, **865**, 86
Temim T., Slane P., Kolb C., Blondin J., Hughes J. P., Bucciantini N., 2015, *ApJ*, **808**, 100
Temim T., Slane P., Raymond J. C., Patnaude D., Murray E., Ghavamian P., Renzo M., Jacovich T., 2022, *arXiv e-prints*, p. [arXiv:2205.01798](#)
Verbunt F., Igoshev A., Cator E., 2017, *A&A*, **608**, A57
Whalen D., van Veelen B., O'Shea B. W., Norman M. L., 2008, *ApJ*, **682**, 49
Wiersma R. P. C., Schaye J., Smith B. D., 2009, *MNRAS*, **393**, 99
Wolfire M. G., McKee C. F., Hollenbach D., Tielens A. G. G. M., 2003, *ApJ*, **587**, 278
de Vries M., et al., 2021, *ApJ*, **908**, 50
van Marle A. J., Meliani Z., Marcowith A., 2015, *A&A*, **584**, A49
van der Swaluw E., 2003, *A&A*, **404**, 939
van der Swaluw E., Achterberg A., Gallant Y. A., Downes T. P., Keppens R., 2003, *A&A*, **397**, 913
van der Swaluw E., Downes T. P., Keegan R., 2004, *A&A*, **420**, 937

This paper has been typeset from a \LaTeX file prepared by the author.